FUTURE SYNCHROTRON LIGHT SOURCES BASED ON ULTIMATE STORAGE RINGS*

Yunhai Cai, SLAC National Accelerator Laboratory, Menlo Park, CA 94025, USA

Abstract

The main purpose of this talk is to describe how far one might push the state of the art in storage ring design. The talk will start with an overview of the latest developments and advances in the design of synchrotron light sources based on the concept of an "ultimate" storage ring. The review will establish how bright a ring based light source might be, where the frontier of technological challenges are, and what the limits of accelerator physics are. Emphasis will be given to possible improvements in accelerator design and developments in technology toward the goal of achieving an ultimate storage ring.

INTRODUCTION

An ultimate storage ring (USR) [1], defined as an electron ring-based light source having an emittance in both transverse planes at the diffraction limit for the range of X-ray wavelengths of interest for a scientific community, would provide very high brightness photons having high transverse coherence that would extend the capabilities of X-ray imaging and probe techniques beyond today's performance. It would be a cost-effective, high-coherence 4th generation light source [2], competitive with one based on energy recovery linac (ERL) technology, serving a large number of users studying material, chemical, and biological sciences. Furthermore, because of the experience accumulated over many decades of ring operation, it would have the great advantage of stability and reliability.

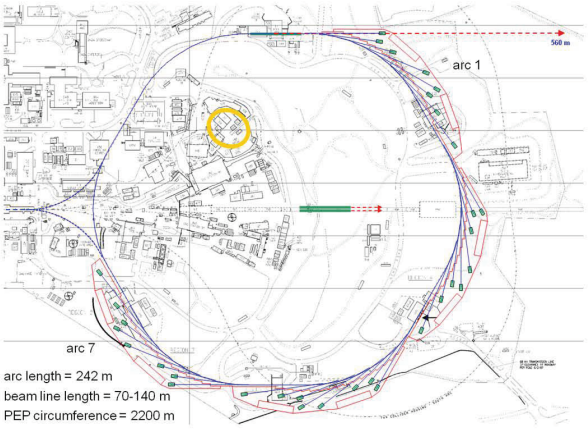

Figure 1: *Layout of PEP-X at SLAC as an ultimate storage ring.*

* Work supported by the Department of Energy under Contract Number: DE-AC02-76SF00515.

In this paper we consider the design of an USR having 10-pm-rad emittance. It is a tremendous challenge to design a storage ring having such an extremely low emittance, a factor of 100 smaller than those in existing light sources, especially such that it has adequate dynamic aperture and beam lifetime. In many ultra-low emittance designs [3, 4, 5], the injection acceptances are not large enough for accumulation of the electron beam, necessitating on-axis injection where stored electron bunches are completely replaced with newly injected ones. Recently, starting with the MAX-IV 7-bend achromatic cell [6], we have made significant progress [7, 8] with the design of PEP-X, a USR that would inhabit the decommissioned PEP-II tunnel at SLAC (Fig. 1). The enlargement of the dynamic aperture is largely a result of the cancellations [9] of the 4th-order resonances in the 3rd-order achromats [10] and the effective use of lattice optimization programs [11, 12].

In this paper, we will show those cancellations of the 4th-order resonances using an analytical approach based on the exponential Lie operators and the Poisson brackets. Wherever possible, our analytical results will be compared with their numerical counterparts [9]. Using the derived formulae, we will construct 4th-order geometric achromats and use them as modules for the lattice of the PEP-X USR, noting that only geometric terms are canceled to the 4th order.

DIFFRACTION LIMITED BRIGHTNESS

The wavelength of synchrotron radiation at the n^{th} harmonic from an electron beam in a planar undulator having a period of λ_u and a peak magnetic field B_0 is given by

$$\lambda_n = \frac{\lambda_u}{2n\gamma^2}(1 + K^2/2), \quad (n = 1, 3, 5, ...) \qquad (1)$$

where γ is the Lorentz relativistic factor and $K = eB_0\lambda_u/2\pi mc$ is the undulator strength parameter. The bandwidth of the spectral line at the n^{th} harmonic is inversely proportional to the product of the number of undulator periods N_u and the harmonic number n,

$$\frac{\Delta\omega}{\omega_n} \approx \frac{1}{nN_u}. \qquad (2)$$

The angle-integrated photon spectral flux in the forward direction is proportional to the electron beam current I and can be written as [13]

$$\mathcal{F}_n = \frac{\pi}{2}\alpha N_u \frac{\Delta\omega}{\omega}\frac{I}{e}Q_n(\frac{nK^2}{4 + 2K^2}). \qquad (3)$$

Here α is the fine structure constant and the function $Q_n(Y)$ is defined by

$$Q_n(Y) = 4Y[J_{(n+1)/2}(Y) - J_{(n-1)/2}(Y)]^2, \qquad (4)$$

Work supported in part by US Department of Energy contract DE-AC02-76SF00515.

Table 1: Main parameters of PEP-X as an ultimate storage ring. The effects of the intra-beam scattering and 90 m of damping wigglers are included.

Parameter	Description	Value
E [GeV]	beam energy	4.5
I [mA]	beam current	200
$\epsilon_{x,y}$ [pm-rad]	x,y emittances	$11.5, 11.5$
σ_δ	energy spread	1.25×10^{-3}
$\beta_{x,y}$ [m]	x,y beta functions at ID	$4.92, 0.8$
λ_u [cm]	period of undulator	2.3
L_u [m]	length of undulator	4.4
K	undulator strength	2.26

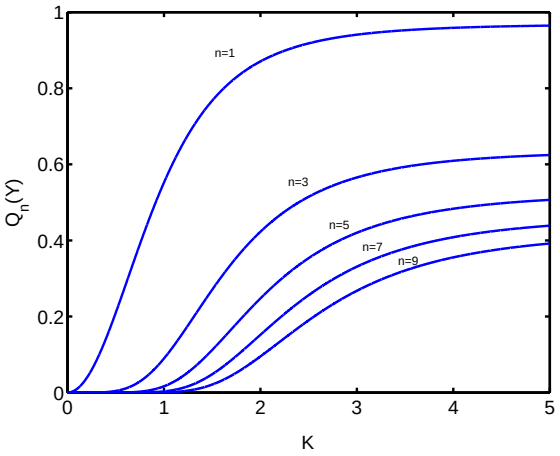

Figure 2: *Function* $Q_n(\frac{nK^2}{4+2K^2})$.

where J_m are the Bessel functions. To achieve a higher flux, one of the important performance parameters for a light source, one needs a higher current, a longer undulator, and a reasonable value of the undulator strength K, as illustrated in Fig. 2. As an example, we calculate the photon spectral flux using the PEP-X parameters in Table 1 and show the results in Fig. 3.

Another important aspect of a light source is its spectral brightness $\mathcal{B}_n$, defined as the ratio of the photon spectral flux to the volume of the convoluted phase of the electron beam and the photon beam in the two transverse dimensions, namely [13],

$$\mathcal{B}_n = \frac{\mathcal{F}_n}{4\pi^2 \Sigma_x \Sigma'_x \Sigma_y \Sigma'_y}, \tag{5}$$

where the convoluted sizes and divergences are

$$\Sigma_{x,y} = \sqrt{\sigma_{x,y}^2 + \sigma_\lambda^2}, \tag{6}$$

$$\Sigma'_{x,y} = \sqrt{\sigma'^2_{x,y} + \sigma'^2_\lambda}. \tag{7}$$

Here $\sigma_{x,y}, \sigma'_{x,y}$ are the RMS sizes and divergences of the electron beam respectively. Given the undulator length

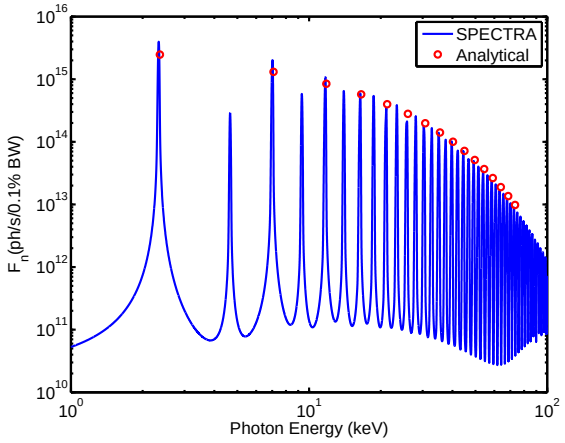

Figure 3: *Photon spectral flux in a 0.1% bandwidth calculated using SPECTRA [14] within the forward cone of* $3\sigma'_{\lambda_1}$ *and the formula (Eq. (3)).*

$L_u = N_u \lambda_u$, the size and divergence of the photon beam are given by

$$\sigma_\lambda = \sqrt{\frac{\lambda_n L_u}{8\pi^2}}, \tag{8}$$

$$\sigma'_\lambda = \sqrt{\frac{\lambda_n}{2L_u}}. \tag{9}$$

It is worth noting that the "emittance" of the photon beam

$$\epsilon_\lambda = \sigma_\lambda \sigma'_\lambda = \lambda_n / 4\pi, \tag{10}$$

depends only on its wavelength. Accordingly, its "beta" function is given by

$$\beta_\lambda = \frac{\sigma_\lambda}{\sigma'_\lambda} = \frac{L_u}{2\pi}. \tag{11}$$

One can easily show that the convoluted phase space area, $2\pi \Sigma_{x,y} \Sigma'_{x,y}$, is at a minimum if the beta functions of the electron beam are matched to those of the photon beam, namely, $\beta_{x,y} = \beta_\lambda$. The matching conditions not only maximize the brightness but also simplify its formula to be

$$\mathcal{B}_n^{(m)} = \frac{\mathcal{F}_n}{4\pi^2 (\epsilon_x + \lambda_n/4\pi)(\epsilon_y + \lambda_n/4\pi)}, \tag{12}$$

where $\epsilon_{x,y}$ are the emittances of the electron beam in the horizontal and vertical planes respectively. Reducing electron emittance increases brightness towards an ultimate upper limit for spontaneous radiation from an undulator:

$$\mathcal{B}_n^{(u)} = \frac{4\mathcal{F}_n}{\lambda_n^2}. \tag{13}$$

While beam brightness can be increased by reducing electron emittance in the denominator of Eq. (12), this emittance reduction may also lead to a reduction in the

achievable flux in the numerator due to collective instabilities in the electron beam. The maximum brightness for angstrom-level spontaneous radiation, the wavelengths of interest for studying the molecular structure and properties of materials, from a particular insertion device in a storage ring is thus due to the trade-off between low emittance and achievable beam current.

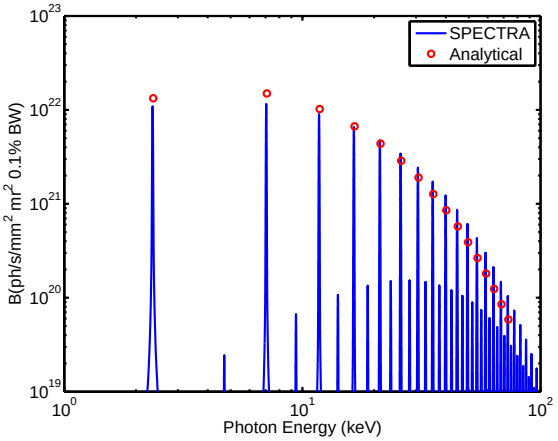

Figure 4: *Spectral brightness of PEP-X at 200 mA, calculated using SPECTRA and the formula (Eq. (5)) multiplying by the reduction factor (Eq. (16)).*

So far, we have ignored the emittance of the electron beam in the longitudinal dimension. Actually, the energy spread of the beam adds to the width of the undulator's spectral lines, thereby reducing spectral brightness. Assuming the electron beam has a Gaussian distribution in the relative energy δ (= dE/E) given by

$$\rho(\delta) = \frac{1}{\sqrt{2\pi}\sigma_\delta} e^{-\frac{\delta^2}{2\sigma_\delta^2}} \tag{14}$$

then the frequency dependence at the n^{th} harmonic is also a narrow Gaussian with a sigma of $\sigma_{\omega_n} = \omega_n/\sqrt{2}nN_u$, which is consistent with Eq. (2). The reduction factor f_δ can then be estimated by

$$f_\delta = \frac{1}{\sqrt{2\pi}\sigma_\delta} \int_{-\infty}^{\infty} e^{-\frac{\Delta\omega_n{}^2}{2\sigma_{\omega_n}^2}} e^{-\frac{\delta^2}{2\sigma_\delta^2}} d\delta, \tag{15}$$

where $\Delta\omega_n = 2\omega_n\delta$, which can be derived from Eq. (1). Carrying out the integral, we obtain

$$f_\delta = \frac{1}{\sqrt{1+8(\sigma_\delta n N_u)^2}}. \tag{16}$$

For a large harmonic number n or a large number of undulator periods N_u, the reduction becomes significant. In a typical electron storage ring having relative energy spread $\sigma_\delta = 0.001$, the degradation of brightness at higher harmonics constrains the useful number N_u of bandwidth-reducing undulator periods to no more than a couple of hundred. Moreover, the energy spread indirectly limits the photon flux since it is proportional to N_u.

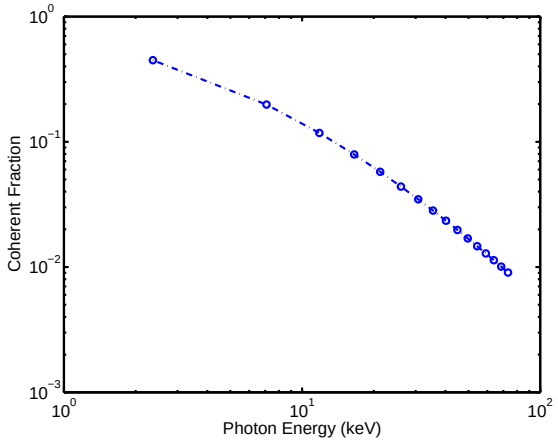

Figure 5: *Coherent fraction for the PEP-X ultimate storage ring.*

To give an example of a synchrotron light source reaching the diffraction limit at 1-Å wavelength, we use the PEP-X parameters tabulated in Table 1 and calculate the spectral brightness as shown in Fig. 4. In the figure, one can see a comparison of the results generated by SPECTRA and the analytical formulas outlined in this section. At the peaks of the odd harmonics, the agreement between the numerical code and the analytical approach is excellent.

Finally, as the emittances approach the diffraction limit, namely $\epsilon_{x,y} \approx \lambda_n/4\pi$, the synchrotron light has more coherence in the transverse dimensions. One can define the fraction of coherence,

$$f_{coh} = \frac{\mathcal{B}_n}{\mathcal{B}_n^{(u)}} = \frac{\lambda_n^2}{16\pi^2\Sigma_x\Sigma_x'\Sigma_y\Sigma_y'}, \tag{17}$$

to quantify the degree of coherence. Using the parameters in Table 1, we calculate the coherent fraction and plot it in Fig 5. One can see that the PEP-X design provides extremely high coherence multi-keV X-rays.

It is clear from the figures of photon flux, spectral brightness, and coherent fraction that PEP-X would be a future light source superior to existing facilities such as PETRA-III [15] or projects under construction [6, 16]. It would also be competitive with the other future light sources [2] based on an ERL.

LATTICE DESIGN

To reach the diffraction limit of angstrom X-rays, the lattice of the PEP-X ultimate storage ring must yield a very low electron emittance, on the order of 10 pm-rad at 4.5 GeV beam energy, while providing dispersion-free optics for insertion devices (IDs) and sufficient dynamic aperture for injection and beam lifetime. An additional constraint is that PEP-X must fit into the existing 2.2-km PEP-II tunnel and therefore must adopt the PEP-II ring layout having

six 243-m long arcs and six 123-m long straight sections as shown in Fig. 1. The PEP-X arcs have identical lattices comprised of periodic cells, and the long straights are made of nearly periodic FODO cells, except in the injection straight. The complete list of PEP-X lattice parameters with 90 m of damping wigglers is shown in Table 2.

Table 2: PEP-X lattice parameters with damping wigglers at zero beam current.

Parameter	Value
Energy, E [GeV]	4.5
Circumference, $\mathcal{C}$ [m]	2199.32
Tune, ν_x, ν_y, ν_s	113.23, 65.14, 0.0069
Emittance, ϵ_{0w} [pm·rad]	11.0
Bunch length, σ_z [mm]	3.0
Energy spread, σ_δ	1.20×10^{-3}
Momentum compaction	4.96×10^{-5}
Damping time, τ_x, τ_y, τ_s [ms]	19, 22, 12
Natural chromaticity, ξ_{x0}, ξ_{y0}	-162.3, -130.1
Energy loss per turn, U_0 [MeV]	2.95
RF voltage, V_{RF} [MV]	8.3
RF frequency, f_{RF} [MHz]	476
Harmonic number	3492
Wiggler length, L_w [m]	89.66
Wiggler period, λ_w [cm]	5.0
Wiggler peak field, B_w [T]	1.5
Length of ID straight, L_{ID} [m]	5.0
Beta at ID center, β_x, β_y [m]	4.92, 0.80

Low Emittance Optics

As a result of the balance between quantum excitation and radiation damping, an electron beam in storage rings reaches an equilibrium distribution with horizontal emittance given by [17],

$$\epsilon_x = C_q \frac{\gamma^2}{I_x} \frac{I_5}{I_2} \tag{18}$$

with

$$C_q = \frac{55}{32\sqrt{3}} \frac{\hbar}{mc}, \quad I_2 = \oint \frac{ds}{\rho^2}, \quad I_5 = \oint \frac{\mathcal{H}_x}{\rho^3} ds, \tag{19}$$

where

$$\mathcal{H}_x = \beta_x \eta_x'^2 + 2\alpha_x \eta_x \eta_x' + \gamma_x \eta_x^2, \tag{20}$$

I_x is the horizontal damping partition number, ρ the bending radius, η_x, η_x' are the horizontal dispersion and its slope, and $\beta_x, \alpha_x, \gamma_x$ the horizontal Courant-Snyder parameters. For a simple ring that has no wigglers, the above dependence can be simplified to a scaling relationship:

$$\epsilon_0 = C_q F \gamma^2 \theta^3 / I_x, \tag{21}$$

where the value of F depends on the type of cell optics, and θ is the dipole bending angle per a cell unit. For a minimal emittance, it is therefore desired to use a large number of short cells with low θ and a type of cell lattice with low F. Note that due to the strong dependence on θ, the rings with longer total arc length have a significant advantage. For comparison, the total length of PEP-X arcs is about 2/3 of the ring circumference, namely 1460 m.

The optics of the so-called theoretical minimum emittance (TME) [18] cell is designed to yield the lowest value of the factor F

$$F_{min}^{(TME)} = \frac{1}{12\sqrt{15}}. \tag{22}$$

and therefore can reach the lowest possible emittance. However, the TME-type cells are not suitable for insertion devices due to lack of dispersion-free straights. On the other hand, double bend achromat [19] (DBA) cells, widely used in light source rings, provide dispersion-free straights for IDs, but their minimal natural emittance is a factor of 3 higher relative to a TME cell with the same bending angle. A compromise solution to obtain both a low emittance and dispersion-free straight is a hybrid cell – the so-called multi-bend achromat (MBA) – comprised of several short TME type units at the cell center and a dispersion matching unit (similar to half DBA) at each cell end.

The compact cell design requires both optical and engineering solutions. An example is the MAX-IV 7-bend achromat cell [6], where the standard TME defocusing quadrupoles are eliminated and replaced by a defocusing gradient in the dipoles, and the sextupole magnets are integrated with dipoles or quadrupoles in compact blocks. A defocusing gradient in the dipole has the added advantage of higher I_x for even lower emittance.

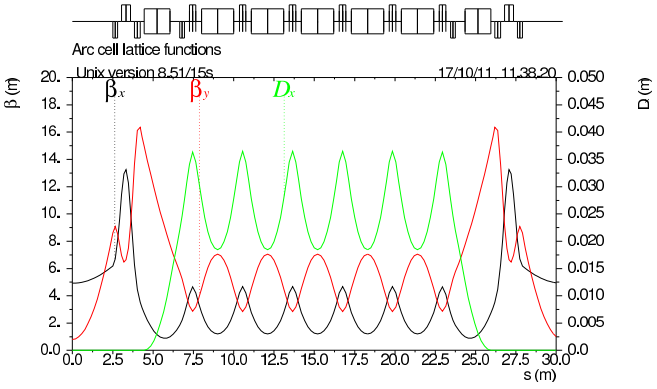

Figure 6: *Lattice functions in PEP-X MBA cell with 7 dipoles.*

The PEP-X MBA cell with 7 dipoles, shown in Fig. 6, is similar to the MAX-IV cell with a few modifications. It has a natural emittance $\epsilon_0 = 29.0$ pm-rad at 4.5 GeV and zero current. The chosen cell phase advance is $\mu_x = 4\pi + \pi/4$ and $\mu_y = 2\pi + \pi/4$ and the cell length is matched to 30.4 m. This provides an optimal linear cell optics and yields 8 cells per arc resulting in an identity linear transformation for each arc. The reason for such a choice will be given in the next section. The TME units have periodic

lattice functions and are made of a focusing quadrupole and a dipole with defocusing gradient per unit. A matching dipole at each cell end is gradient-free and 20% shorter than the TME dipole. The ID straight length is $L_{ID} = 5$ m, and $\beta_x/\beta_y = 4.9/0.8$ m at the ID center. The β_y at ID is near its optimal value of $L_u/2\pi$ for maximum brightness. Compared to MAX-IV, this cell has 4 additional matching quadrupoles for a larger tuning range of the ID β functions. In particular, the ID β_y can be varied up to a 5-m value while the cell phase advance is fixed and the ID β_x and cell emittance are not significantly changed.

An ultra-low emittance lattice such as that of PEP-X is characterized by very small beta functions and dispersion, achieved with many quadrupoles and resulting in very large natural chromaticity. To correct the chromaticity, the chromatic sextupole magnets become extremely strong as the dispersion gets smaller and smaller. The nonlinear effects generated by such strong sextupoles result in a severe reduction of dynamic aperture. An efficient minimization of these nonlinearities becomes essential for a successful design of an ultimate storage ring.

The cell sextupole scheme consists of 4 families of chromatic sextupoles and 6 harmonic sextupoles. The chromaticity-correcting sextupoles are placed at the center of the TME focusing quadrupoles and at each end of the dipole where dispersion is not zero. The harmonic sextupoles are placed within the two dispersion-free quadrupole triplets adjacent to the ID straight. This scheme provides sufficient flexibility for optimization of nonlinear chromaticity and amplitude dependence of the betatron tunes from the sextupole perturbations.

The cell magnet parameters are within a reasonable range. At 4.5 GeV, the dipole field is <1.5 kG, the quadrupole field is <8.6 kG at 20 mm radius, and the sextupole field is <7.8 kG at 15 mm radius and 0.2 m sextupole length.

Perturbation of Sextupoles

We would like to provide a general treatment of sextupole perturbation and then apply it to the design of PEP-X. For simplicity, we start with the geometric abberations. Let us consider a set of thin-lens sextupoles at position $i = 1, ..., n$ in a beamline. Between any two adjacent sextupoles at positions $i-1$ and i, we have a linear transfer map $\mathcal{M}_{i-1,i}$. Based on the Lie algebra method [20], the transfer map $\mathcal{M}$ of the beamline can be written as [21]

$$\mathcal{M} = \mathcal{M}_{0,1} e^{-:\mathcal{V}_1(\vec{z}):} ... \mathcal{M}_{n-1,n} e^{-:\mathcal{V}_n(\vec{z}):} \mathcal{M}_{n,n+1}, \quad (23)$$

where $\vec{z}$ is a vector in the four-dimensional transverse phase space and the vector potential $\mathcal{V}_i(\vec{z}) = S_i(x^3 - 3xy^2)/6$. Here we have denoted S_i as an integrated strength,

$$S_i = \frac{L_i}{(B\rho)} \frac{\partial^2 B_y}{\partial x^2}, \quad (24)$$

where L_i is the length of the sextupole magnet and $(B\rho)$ the magnetic rigidity. By repeatedly applying a similarity transformation,

$$\mathcal{L}^{-1} e^{-:\mathcal{F}(\vec{z}):} \mathcal{L} = e^{-:\mathcal{F}(\mathcal{L}^{-1}\vec{z}):}, \quad (25)$$

where $\mathcal{L}$ is a linear map and $\mathcal{F}$ is an arbitrary function, one can show [21]

$$\mathcal{M} = \mathcal{M}_{0,n+1} e^{-:\mathcal{V}_1(\mathcal{M}^{-1}_{1,n+1}\vec{z}):} ... e^{-:\mathcal{V}_n(\mathcal{M}^{-1}_{n,n+1}\vec{z}):}, \quad (26)$$

where $\mathcal{M}_{i,n+1} = \mathcal{M}_{i,i+1} ... \mathcal{M}_{n,n+1}$ is the linear transfer map from position i to $n+1$ and the superscript "-1" is used to denote its inverse map. One can see from Eq. (26) that the total map $\mathcal{M}$ is factorized into the linear map $\mathcal{M}_{0,n+1}$ and a nonlinear map,

$$e^{-:\mathcal{V}_1(\mathcal{M}^{-1}_{1,n+1}\vec{z}):} ... e^{-:\mathcal{V}_n(\mathcal{M}^{-1}_{n,n+1}\vec{z}):}; \quad (27)$$

and more importantly all nonlinearities are effectively transported to the end of the beamline.

It is well known that one can use a linear symplectic map $\mathcal{A}^{-1}$ to make a coordinate transformation to the normalized coordinates. As a consequence, the linear transfer map can be decomposed into $\mathcal{M}_{i,n+1} = \mathcal{A}_i^{-1} \mathcal{R}_{i,n+1} \mathcal{A}_{n+1}$, where $\mathcal{R}_{i,n+1}$ is a rotational map with the betatron phase advances $\mu_{x,i}, \mu_{y,i}$ as the angles. Using the normalized coordinates and repeatedly applying the similarity transformation (Eq. (25)), we can rewrite the map of the beamline as

$$\mathcal{M} = \mathcal{A}_0^{-1} \mathcal{R}_{0,n+1} e^{-:\mathcal{V}_1(\mathcal{R}^{-1}_{1,n+1}\mathcal{A}_1\vec{z}):} ... \\ e^{-:\mathcal{V}_n(\mathcal{R}^{-1}_{n,n+1}\mathcal{A}_n\vec{z}):} \mathcal{A}_{n+1}. \quad (28)$$

Explicitly, we have

$$\mathcal{V}_i(\mathcal{R}^{-1}_{i,n+1}\mathcal{A}_i\vec{z}) = \frac{S_i\sqrt{\beta_{x,i}}}{6}(\beta_{x,i}x_i^3 - 3\beta_{y,i}x_i y_i^2), \quad (29)$$

where $\beta_{x,i}, \beta_{y,i}$ are the optical beta functions at position i, $x_i = x\cos\mu_{x,i} - p_x \sin\mu_{x,i}$, and $y_i = y\cos\mu_{y,i} - p_y \sin\mu_{y,i}$. In fact, x_i, y_i are the normalized coordinates respectively in the horizontal and vertical planes at position i.

So far, we have not yet made any approximations. To carry out the perturbation theory of the sextupoles, we need to combine the Lie factors $e^{-\mathcal{V}_1} ... e^{-\mathcal{V}_n}$ in Eq. (28) into a single Lie operator. This can be achieved by repeatedly applying the Cambell-Baker-Hausdorf theorem $e^{:\mathcal{A}:} e^{:\mathcal{B}:} = e^{:\mathcal{C}:}$, where $\mathcal{C} = \mathcal{A} + \mathcal{B} + \{\mathcal{A}, \mathcal{B}\}_{PB}/2 + ...$ Here the bracket with the subscript "PB" denotes the well-known Poisson Bracket. for the perturbation of the sextupole strength S, we obtain

$$\mathcal{M} = \mathcal{A}_0^{-1} \mathcal{R}_{0,n+1} e^{:f_3 + f_4 + ...:} \mathcal{A}_{n+1}, \quad (30)$$

where

$$f_3 = -\sum_{i=1}^{n} \mathcal{V}_i \quad (31)$$

and

$$f_4 = \frac{1}{2} \sum_{i=1}^{n} \sum_{j>i}^{n} \{\mathcal{V}_i, \mathcal{V}_j\}_{PB}. \quad (32)$$

Clearly, f_3 is of the first order of S and f_4 of the second order. Similar to the Hamiltonian perturbation theory, f_3 gives the driving term of the third-order resonances provided that the action-angle variables, $x = \sqrt{2J_x}\cos\phi_x, p_x = -\sqrt{2J_x}\sin\phi_x, y = \sqrt{2J_y}\cos\phi_y$, and $p_y = -\sqrt{2J_y}\sin\phi_y$ are used.

The Poisson bracket of any pair of $\mathcal{V}_{i,j}$ can be computed easily and the result is given by

$$\begin{aligned}&\{\mathcal{V}_i, \mathcal{V}_j\}_{PB} = S_i S_j \sqrt{\beta_{x,i}\beta_{x,j}}\\ &\times[\sin(\mu_{y,i} - \mu_{y,j})\beta_{y,i}\beta_{y,j}x_i x_j y_i y_j\\ &+\sin(\mu_{x,i} - \mu_{x,j})(\beta_{x,i}x_i^2 - \beta_{y,i}y_i^2)\\ &\times(\beta_{x,j}x_j^2 - \beta_{y,j}y_j^2)/4]. \end{aligned} \quad (33)$$

Clearly, all terms in the brackets are octupole like, namely a fourth-order monomial in x, p_x, y and p_y. It is worth noting that this bracket vanishes when the phase differences in both planes are integers of π.

Essentially, we have worked out the first and, more importantly, the second order sextupole perturbation using the Lie method. Our assumption of a thin lens could be removed since one can always divide a thick sextupole into many thin slices and then apply the thin-lens formulas. In practice, it is sometimes easier to compute [9] f_3 and f_4 numerically using the differential algebra [22] and Dragt-Finn factorization [23].

A Family of Sextupoles in Arc

Now we can apply the general results of the perturbation theory to the arcs of PEP-X. As we mentioned in a previous section, we designed a periodical cell with betatron phase advances, $\mu_x = 4\pi + \pi/4$ and $\mu_y = 2\pi + \pi/4$, in the horizontal and vertical planes respectively. For the linear optics, every eight of such cells makes an identity transformation and form an achromat. In the design lattice, every arc consists of one such achromat. We would like to explain why this choice was made.

Let us study an achromat that consists of eight PEP-X cells and each cell has a thin sextupole at the same location. It is well known that $f_3 = 0$ in the achromat [10]. This can also be shown directly using Eqs. (29) and (31). As a result, this beamline preserves the property of an achromat, even at a nonlinear level, up to the first order of sextupole strength.

To proceed to the next order, we need to compute f_4 using Eqs. (32) and (33) and add up the contributions from all 28 brackets. Expressing the result in terms of the complex coordinates, $x = (a_x + ia_x^+)/\sqrt{2}, p_x = (ia_x + a_x^+)/\sqrt{2}, y = (a_y + ia_y^+)/\sqrt{2}, p_y = (ia_y + a_y^+)/\sqrt{2}$, we have

$$\begin{aligned} f_4 \;=\; & -\frac{1}{4}S^2\beta_x\{(1+2\sqrt{2})[\beta_x^2(a_x a_x^+)^2 + \beta_y^2(a_y a_y^+)^2]\\ & -4\beta_y[(1+\sqrt{2})\beta_x - \sqrt{2}\beta_y](a_x a_x^+)(a_y a_y^+)\\ & +\beta_y[\beta_x + 2(1+\sqrt{2})\beta_y]\\ & \times[e^{-2i(\psi_x-\psi_y)}(a_x)^2(a_y^+)^2\\ & +e^{2i(\psi_x-\psi_y)}(a_x^+)^2(a_y)^2]\}, \end{aligned} \quad (34)$$

where ψ_x and ψ_y are the phase advances from the last sextupole to the end of the achromat. One can easily see, by using action-angle variables $a_x = \sqrt{J_x}e^{i\phi_x}$, $a_x^+ = -i\sqrt{J_x}e^{-i\phi_x}$, $a_y = \sqrt{J_y}e^{i\phi_y}$, and $a_y^+ = -i\sqrt{J_y}e^{-i\phi_y}$, that there are three tune shift terms and a single resonance driving term: $2\nu_x - 2\nu_y$. The other resonances, $4\nu_x, 4\nu_y, 2\nu_x, 2\nu_y$, and $2\nu_x + 2\nu_y$, are canceled out among the eight sextupoles.

A Fourth-Order Geometric Achromat

Recently, we used the lattice design code OPA [11] to optimize the settings of 10 sextupole families. Due to the cancellations of most resonances, we only needed to control the nonlinear chromaticities up to the second order, the three remaining amplitude-dependent tune shifts, and the residual $2\nu_x - 2\nu_y$ resonance. A good solution with small nonlinearities was found [8]. The derivatives of the betatron tunes are calculated using the normal form method [24] and tabulated in Table 3 along with a new solution based on 4th-order achromats ($f_3 = f_4 = 0$). As one can see from the table, the tune shift terms are significantly reduced using the 4th-order achromats without any degradation in the chromatic parts. The small residuals are due to the nonlinear kinematic terms in the Hamiltonian.

Table 3: The nonlinear chromaticities and tune shifts due to betatron amplitudes in the PEP-X ultimate storage ring.

Derivatives of tunes	4th-order achromats
$\partial\nu_{x,y}/\partial\delta$	$0, 0$
$\partial^2\nu_{x,y}/\partial\delta^2$	$-57, -89$
$\partial^3\nu_{x,y}/\partial\delta^3$	$+1332, -150$
$\partial\nu_x/\partial J_x\ [m^{-1}]$	$+253$
$\partial\nu_{x,y}/\partial J_{y,x}\ [m^{-1}]$	$+1158$
$\partial\nu_y/\partial J_y\ [m^{-1}]$	-228

As outlined in the previous section, one can compute all contributions to f_4 from all families of sextupoles by using Eq. (34) and a similar expression for the crossing term [25] between two sextupole families. To find a 4th-order geometric achromat, we simply adjusted the strengths of six families of the harmonic sextupoles to eliminate the five non-vanishing terms in f_4. In fact, we have an infinite set of solutions which can be found by searching numerically using the Nelder-Mead method. We use the extra degree of freedom to minimize the peak value of the harmonic sextupoles. As a result, the peak strength is reduced by 25% from the OPA solution. All terms in f_3 and f_4 are plotted as a function of the position along one of the arcs in PEP-X in Fig. 7. One can see from the figures that the numerical calculations using the actual beamline confirm the analytical results. Although we have not analyzed the chromatic effects in this paper, in fact both the first- and second-order dispersions are also canceled within this achromat as shown in reference [10].

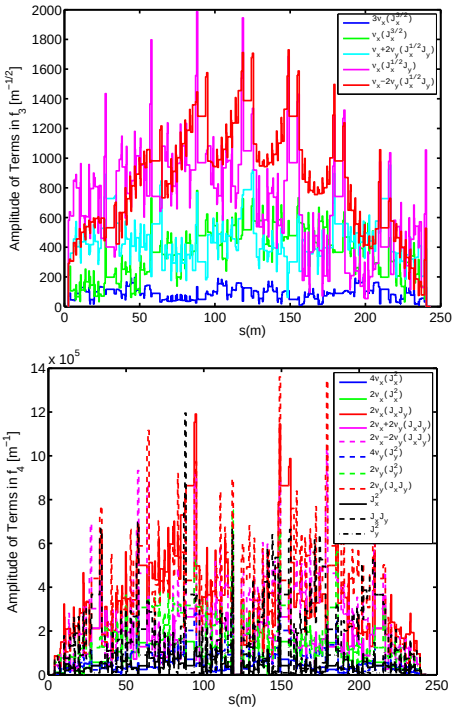

Figure 7: *All 3rd-order resonance terms in f_3 (top) and all 4th-order resonance as well as three tune shift terms in f_4 (bottom) generated by the 10 families of sextupoles as they accumulated in the PEP-X achromat.*

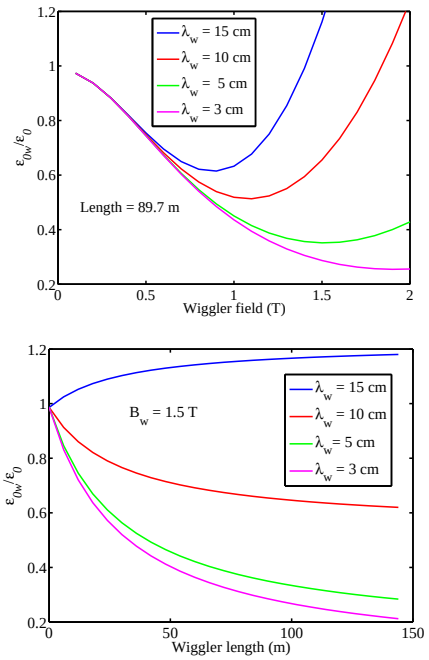

Figure 8: *Relative emittance reduction versus wiggler field (top) and versus wiggler length (bottom) for various values of wiggler period.*

Damping Wiggler

Because the emittance of PEP-X will increase by a factor of 2 from the zero-current natural value of 29 pm-rad achieved with the 7BA lattice due to intra-beam scattering with 200-mA stored beam current (Section 5), a further reduction in emittance by about a factor of three is needed to reach the diffraction limit for 1-Å X-rays (assuming 100% horizontal-vertical emittance coupling). This emittance reduction can be achieved using one or more strong damping wigglers in one or more dispersion-free regions.

The relative reduction in natural emittance from ϵ_0 to ϵ_{w0} caused by a damping wiggler in PEP-X can be estimated using an approximate analytical expression [26]:

$$\frac{\epsilon_{0w}}{\epsilon_0} = (\frac{I_{x0}}{I_{xw}}) \frac{1 + \frac{4C_q}{15\pi I_{x0}} N_p \gamma^2 \frac{<\beta_{xw}>\rho_o}{\epsilon_{x0}\rho_w^2}\theta_w^3}{1 + \frac{1}{2} N_p \frac{\rho_o}{\rho_w}\theta_w}, \qquad (35)$$

where I_{xw}, I_{x0} are damping partition numbers with and without wigglers, N_p is the number of wiggler periods, $< \beta_{xw} >$ the average horizontal β-function in the wiggler, ρ_w the bending radius at peak wiggler field, $\theta_w = \lambda_w/2\pi\rho_w$ and λ_w the wiggler period length. Here $\rho_o = \rho_c\rho_m/(r\rho_c + (1-r)\rho_m)$ is the effective bending radius in the MBA cell, with ρ_c and ρ_m being the bending radii in the main cell dipole and the matching dipole, respectively, and r being the relative contribution from the matching dipoles to the total bending angle.

It follows that the emittance reduction depends on the wiggler period length, the wiggler peak field, and the total wiggler length. Using Eq. (35), Fig. 8 shows the ratio of ϵ_{0w}/ϵ_0 versus the wiggler peak field and the total wiggler length for various values of wiggler period length, where the wiggler is inserted in a long straight section with $< \beta_x > = 12.4$ m. One can see that most of the damping occurs within 100 m of the wiggler length, and that a wiggler period below 5 cm does not significantly improve the damping. Selecting a 90-m long wiggler with a 5-cm period, it follows that the optimal peak field is 1.5 T. It should be noted that a short 5-cm wiggler period implies a small wiggler gap of 7.7 mm when using a hybrid magnet design [27]. A wiggler with the above parameters has been modeled in the lattice using an array of alternating field short dipoles. The wiggler is placed in one 123-m long FODO straight section, where it is split into 18 sections to fit between the quadrupoles. The resultant emittance with wigglers at zero current is $\epsilon_{0w} = 11$ pm-rad.

The damping wiggler creates various negative effects on the PEP-X beam. It increases the beam rms energy spread from 0.072% to 0.12%, and the radiation loss per turn from 0.36 MeV to 2.95 MeV. The latter amounts to a 0.59 MW at 200 mA current. Finally, the wiggler field has intrinsic nonlinear components on the beam trajectory affecting large amplitude particles.

DYNAMIC APERTURE

Ultimately, the goal of minimizing sextupole non-linear aberrations is to maximize the PEP-X dynamic aperture for efficient horizontal injection and long beam lifetime. The

dynamic aperture was obtained in particle tracking simulations using LEGO [28]. The calculations included on-momentum and off-momentum particles and magnet errors. To include the effects of the intrinsic non-linear wiggler field, the 1st order dipole wiggler model was replaced by an exact non-linear field wiggler model in the simulations.

Error-Free Aperture

To verify the effect of residual sextupole aberrations, dynamic apertures for the 4th-order geometric achromat solution was evaluated without magnet errors and with momentum error δ up to 2%, as shown in Fig. 9.

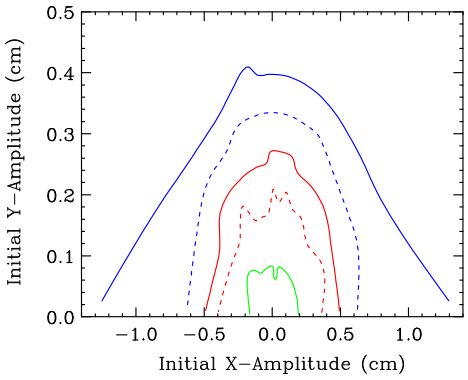

Figure 9: *Dynamic aperture of the bare lattice.*

Error Tolerances

Magnet field and alignment errors create linear and non-linear optics perturbations. These include distortion of the closed orbit and betatron functions, transverse coupling, chromaticity, variation of betatron tune with amplitude and excitation of betatron resonances leading to reduced dynamic aperture. To maintain a sufficient aperture, the ring must include efficient correction schemes; also, the magnitude of such errors must be limited to an acceptable level. To estimate the error sensitivities for the PEP-X lattice with the 4th-order achromat sextupole solution, LEGO tracking simulations were performed.

LEGO simulations included realistic correction of orbit, beta beat, linear chromaticity and vertical dispersion. A suitable coupling correction procedure has not yet been implemented in the code; therefore the studied errors were limited to magnet field errors, horizontal misalignment and higher order multipole field errors. The latter were based on the measured field in the PEP-II magnets but applied to the smaller bore radius of the PEP-X magnets. No errors were applied to beam position monitors, and the linear chromaticity was adjusted to +1.

It was found that rms horizontal misalignment of 20 μm and relative rms field error of 10^{-3} in dipoles, quadrupoles and sextupoles are acceptable. Dynamic apertures with the above errors, including the high-order multipole field errors for 10 random settings after correction, are shown in

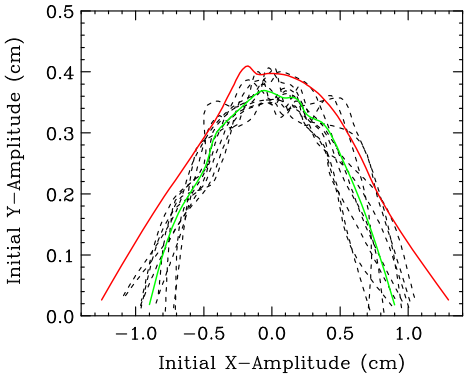

Figure 10: *Dynamic aperture with machine errors.*

Fig. 10. Here, the average on-momentum horizontal dynamic aperture is 9 mm which is sufficient for off-axis injection assuming a high quality injected beam with a 1 μm-rad normalized emittance and an effective septum width of 3 mm. It should be noted that a smaller dynamic aperture could still be accommodated using on-axis injection.

IBS AND TOUSCHEK LIFETIME

Intra-beam scattering (IBS) describes multiple Coulomb scattering that leads to growth in emittance and energy spread in electron machines, whereas the Touschek effect concerns large single Coulomb scattering events where energy transfer from transverse to longitudinal planes leads to particle loss. In low emittance machines such as PEP-X, both effects are important.

Intra-beam scattering

For our IBS calculations we assume that the lattice is coupling-dominated, by which we imply that the vertical dispersion can be kept sufficiently small. Then the vertical emittance is proportional to the horizontal emittance, and we write

$$\epsilon_x = \frac{\epsilon}{1+\kappa} \qquad \text{and} \qquad \epsilon_y = \frac{\kappa\epsilon}{1+\kappa}\,, \tag{36}$$

with κ being the coupling constant between 0 and 1 and $\epsilon = \epsilon_x + \epsilon_y$ being the sum emittance at finite current with IBS. The nominal (no IBS) horizontal and vertical emittances are given by $\epsilon_{x0} = \epsilon_{0w}/(1+\kappa)$ and $\epsilon_{y0} = \kappa\epsilon_{0w}/(1+\kappa)$, where ϵ_{0w} is the natural emittance with the damping wigglers at zero current and its value is given in Table 2.

For the steady-state, the sum emittance ϵ and the energy spread σ_δ are given by

$$\epsilon = \frac{\epsilon_{0w}}{1-\tau_x^*/T_x} \qquad \text{and} \qquad \sigma_\delta^2 = \frac{\sigma_{\delta w}^2}{1-\tau_s/T_p}\,, \tag{37}$$

where $\tau_x^* = \tau_x/(1+\kappa\tau_x/\tau_y)$. The quantities $\sigma_{\delta w}$, τ_s, and $1/T_p$ signify, respectively, the nominal beam size, the radiation damping time, and the IBS growth rate in momentum.

A simplified model of the B-M equations [29] that can be used (with slight modification) to approximate the results for PEP-X is the so-called "high energy approximation" [30]. We present it here since it relatively clearly shows the parameter dependence of IBS, though to obtain the numerical results for PEP-X (given below) we will use the more accurate B-M equations. According to this simplified model the IBS growth rate in energy spread is given by

$$\frac{1}{T_p} \approx \frac{r_e^2 c N_b (\log)}{16\gamma^3 \epsilon_x^{3/4}\epsilon_y^{3/4}\sigma_z\sigma_\delta^3}\left\langle \sigma_H\, g(\alpha)\, (\beta_x\beta_y)^{-1/4}\right\rangle \ . \tag{38}$$

Here r_e is the classical radius of the electron, N_b the number of electrons per bunch, $(\log)$ the Coulomb log factor, σ_z the bunch length, and β_x and β_y the optical beta functions. Other factors in Eq. (38) are defined by

$$\frac{1}{\sigma_H^2} = \frac{1}{\sigma_\delta^2} + \frac{\mathcal{H}_x}{\epsilon_x}\ , \quad \alpha = \sqrt{\frac{\beta_x\epsilon_y}{\beta_y\epsilon_x}}\ , \tag{39}$$

$$g(\alpha) = \alpha^{(0.021 - 0.044\ln\alpha)}\ , \tag{40}$$

with $\mathcal{H}_x$ the dispersion invariant defined in Eq. (20).

In the high energy approximation, the horizontal IBS growth rate is given in terms of the momentum growth rate simply as

$$\frac{1}{T_x} = \frac{\sigma_\delta^2}{\epsilon_x}\langle \mathcal{H}_x \delta(1/T_p)\rangle\ . \tag{41}$$

We see that only the arcs contribute significantly to IBS-induced emittance growth, since only in the arcs is $\mathcal{H}_x$ non-zero. Note that $\langle\delta(1/T_p)\rangle = 1/T_p$, where $\langle\rangle$ means to average around the ring. Given the growth rates, the steady-state ϵ qnd σ_δ are obtained by solving Eqs. (37) simultaneously. Since the growth rates depend on the beam emittances, energy spread, and bunch length, Eqs. (37) are solved by iteration using a Newton's method.

In scattering calculations like IBS, a Coulomb log term, (log) in Eq. (38), is often used to take into account the contribution of very large and very small impact parameter events. Due to the small impact parameter events, the tails of the steady-state bunch distributions are not Gaussian and the standard way of computing (log) overemphasizes their importance. To better represent the size of the bunch core, we adjust (log) to cut away events with growth rate greater than the synchrotron damping rate, as was proposed by Raubenheimer [31]. For PEP-X, (log) becomes ≈ 11.

For our IBS calculations for PEP-X using lattice parameters found in Table 2, we assume the vertical emittance is given by coupling with $\kappa = 1$. The results of our IBS calculations for the PEP-X lattice at the nominal $I = 200$ mA with the number of bunches $M = 3300$, which corresponds to 0.5 nC bunch charge. The steady-state emittances, energy spread, and bunch length in the normal design have been shown in Table 1. We note that for PEP-X, IBS has little effect on σ_δ and σ_z; however, at the nominal current ϵ_x is double the zero-current value.

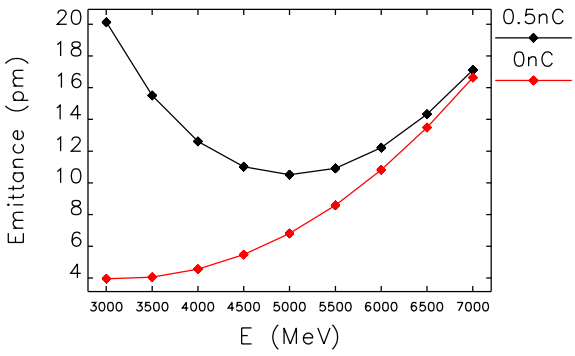

Figure 11: *Emittance $\epsilon_x = \epsilon_y$ vs. energy for a round beam at nominal bunch current (black) and at zero current (red).*

Finally, to demonstrate that 4.5 GeV is near the optimal energy for our lattice, we have performed IBS calculations for different energies. Note that the lattice is scalable with energy except in the wiggler and undulator regions which are assumed to have nominally fixed-field magnets. In Fig. 11 we plot emittance $\epsilon_x = \epsilon_y$ *vs.* electron energy E; we see that the emittance minimum is broad, and that the minimum is near our nominal energy.

Touschek lifetime

Touschek lifetime calculations normally follow the flat-beam equation of Brück [32], with modifications by Piwinski [26]. For round beam calculations we will begin here with the more general formula (*i.e.* not limited to flat beams) due to Piwinski [26, 33]. With the Touschek effect the number of particles in a bunch decays with time t as

$$N_b = \frac{N_{b0}}{1 + t/\mathcal{T}}\ , \tag{42}$$

with N_{b0} the initial bunch population, and $\mathcal{T}$ the Touschek lifetime. Note that the decay is not exponential. The lifetime is given by [26]

$$\frac{1}{\mathcal{T}} = \frac{r_e^2 c N_b}{8\sqrt{\pi}\beta^2\gamma^4\sigma_z\sigma_\delta\epsilon_x\epsilon_y}\left\langle \sigma_H \mathcal{F}(\delta_m)\right\rangle\ , \tag{43}$$

with

$$\begin{aligned}\mathcal{F}(\delta_m) &= \int_{\delta_m^2}^{\infty}\frac{d\tau}{\tau^{3/2}} e^{-\tau B_+} I_0(\tau B_-) \\ &\times \left[\frac{\tau}{\delta_m^2} - 1 - \frac{1}{2}\ln\left(\frac{\tau}{\delta_m^2}\right)\right]\ ,\end{aligned} \tag{44}$$

$$B_\pm = \frac{1}{2\beta^2\gamma^2}\left|\frac{\beta_x\sigma_x^2}{\epsilon_x\tilde{\sigma}_x^2} \pm \frac{\beta_y}{\epsilon_y}\right|\ , \tag{45}$$

where σ_H is defined in Eq. (39), and again $\langle\rangle$ indicates averaging around the ring. In this formula the only assumptions are that there is no vertical dispersion and that the energies are non-relativistic in the beam rest frame ($\gamma^2\sigma_x^2/\beta_x^2$, $\gamma^2\sigma_y^2/\beta_y^2 \ll 1$); there is no requirement that the beam be flat. Parameters are average velocity over the speed of light

β, modified Bessel function of the first kind I_0, relative momentum acceptance δ_m (half aperture), and beam sizes $\sigma_x = \sqrt{\beta_x \epsilon_x + \eta_x^2 \sigma_\delta^2}$ and $\tilde{\sigma}_x = \sqrt{\beta_x \epsilon_x + \beta_x \mathcal{H}_x \sigma_\delta^2}$.

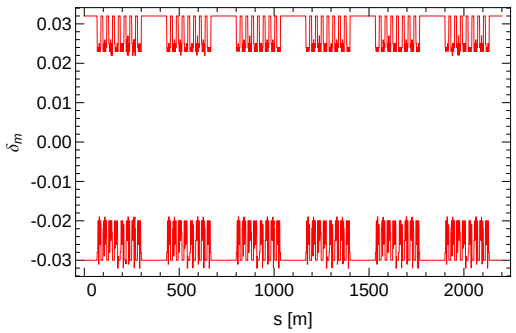

Figure 12: *The momentum acceptance, δ_m, for PEP-X. This function is used in finding the Touschek lifetime.*

We have calculated the momentum aperture as a function of location in PEP-X in the following manner. In tracking, at a given position s, a beam particle is given a relative (positive) momentum kick δ_m, and it undergoes betatron oscillation. The largest value of δ_m for which the particle survives defines the positive momentum aperture at position s. Then the same is done for a negative momentum kick. The results are given in Fig. 12. Using the calculated $\delta_m(s)$ (Fig. 12) and Eq. (43), we obtain the lifetime $\mathcal{T} = 11$ hrs.

CONCLUSION

In this paper, we have most significantly developed a systematic method based on 4th-order geometric achromats to design an USR where the sextupole magnets are the dominant sources of the nonlinearity. One may choose a different achromat for the design of the lattice; however, our methodology is still applicable. In fact, we know that there are many similar solutions of 4th-order achromats. Since they are not quite relevant to the design of PEP-X, we chose not to present them in this paper.

To make a 4th-order geometric achromat, we chose to eliminate all three tune shift terms in the Lie generator f_4. In general, this choice may not be suitable for other lattices. Our method can be easily modified to have any values of those three terms. This will allow us to have full control of the size and orientation of the beam footprint in the tune space of the transverse dimensions.

Our design of the PEP-X USR utilizes the existing PEP-II tunnel, its high power and low emittance injector, and much of the PEP-II RF system. Perhaps most importantly, the design does not rely on new technology developments and is therefore essentially ready to be built.

ACKNOWLEDGMENT

It has been great pleasure working on the PEP-X USR with my SLAC colleagues: Karl Bane, Robert Hettel, Yuri Nosochkov, and Min-Huey Wang. I would like to also thank Michael Borland from ANL for his tremendous efforts and critical contributions in this study.

REFERENCES

[1] M. Bei et al., Nucl. Inst. Meth., A622:518-535, 2010.

[2] G. Hoffstaetter et al., Technical report, Cornell, April 2011.

[3] P. Elleaume and A. Ropert, Nucl. Inst. Meth., A500:18-24, 2003.

[4] K. Tsumaki and N.K. Kumagai, Nucl. Inst. Meth., A565:394-405, 2006.

[5] M. Borland, In Proc. SRI09, Melbourne 2009 AIP Conference Proc., volume 1234, page 911, 2010.

[6] S.C. Leemann et al., Phys. Rev. ST Accel. Beams, 12:120701, 2009.

[7] Y. Nosochkov et al., In Proc. of IPAC2011, San Sebastian, Spain, pages 3068-3070, 2011.

[8] M.-H. Wang et al. In Proc. of IPAC2011, San Sebastian, Spain, page 3065-3067, 2011.

[9] Y. Cai, Nucl. Inst. Meth., A465:168-174, 2011.

[10] K.L. Brown and R.V. Servranckx, Nucl. Inst. Meth., A258:480-502, 1987.

[11] A. Streun, OPA lattice design code..

[12] M. Borland, APS LS 319, Argonne, August 2010.

[13] K.-J. Kim, In AIP Proc. volume 184, pages 565-632, 1989.

[14] T. Tanaka and H. Kitamura, Journal of Synchrotron Radiation, 8:1221-1228, 2001.

[15] K. Balewski at al., Technical design report, DESY 2004-035, DESY, February 2004.

[16] J. Ablett et al., Technical report, Brookhaven.

[17] M. Sands, SLAC 121, SLAC, November 1970.

[18] L.C. Teng, Fermilab Report TM-1269, Fermilab, June 1984.

[19] M. Sommer, LAL/RT/83-15, LAL, November 1983.

[20] A.J. Dragt, J. Opt. Soc. Am., 72-372, 1982.

[21] J. Irwin, Nucl. Inst. Meth., A298:460-472, 1990.

[22] M. Berz, Particle Accelerators, 24:109, 1989.

[23] A.J. Dragt and J.M. Finn., J. Math. Phys. 17:2215-2227, 1976.

[24] M. Berz, E. Forest and J. Irwin, Particle Accelerators, 24:91, 1989.

[25] Y. Cai et al., SLAC-PUB-14785, SLAC, December 2011.

[26] A. Chao and M. Tigner, editors, Word Scientific, 2006. 3rd Printing.

[27] K. Halbach, Journal de Physique, 44:C1-211-216, 1983.

[28] Y. Cai et al. SLAC-PUB-7642, SLAC, August 1997.

[29] J.D. Bjorken and S.K. Mtingwa, Particle Accelerators 13:115-143, 1983.

[30] K. Bane, In Proc. of EPAC2002, Paris, France, pages 1443-1445, 2002.

[31] T. Raubenheimer, Particle Accelerators, 45:111-118, 1994.

[32] H. Brück, "Accélérateurs Circulaires de Particules; introduction à la théorie," Saclay, 1966.

[33] A. Piwinski, DESY 98-179, DESY, November 1998.